Inorganic Chemistry Communications 157 (2023) 111276

Contents lists available at ScienceDirect

Inorganic Chemistry Communications

journal homepage: www.elsevier.com/locate/inoche

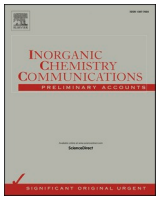

Short communication

Surface modified ZnO nano structures: Electrochemical studies for energy applications and removal of emerging organic pollutant dye by photo induced hetero-catalysis

M. Fazal Ur Rehman [a,b], Manzar Zahra [b], Waseem Shoukat [c], Ali H. Reshak [d,e,f], Dania Ali [g], Aoun Raza [b], Sabeen Arshad [h,i], Muhammad M. Ramli [e]

[a] Energy and Electronics Materials Laboratory, Department of Polymer Engineering, Chonnam National University, Gwangju-61186, Republic of Korea
[b] Department of Chemistry, Lahore Garrison University, Lahore, Pakistan
[c] Institute of Chemical Sciences, Bahauddin Zakariya University, Multan 60800, Pakistan
[d] Physics Department, College of Science, University of Basrah, Basrah 61004, Iraq
[e] Center of Excellence Geopolymer and Green Technology (CEGeoGTech), University Malaysia Perlis, 01007 Kangar, Perlis, Malaysia
[f] Department of Instrumentation and Control Engineering, Faculty of Mechanical Engineering, CTU in Prague, Technicka 4, 616607 Prague, Czech Republic
[g] Faculty of Medicine, Charles University, Pilsen 30100, Czech Republic
[h] Department of Nanoscience, Rovira I Virgili University, Tarragona, Spain
[i] Department of Chemistry, The Government Sadiq College University, Bahawalpur, Pakistan

ARTICLE INFO

Keywords:
Surface modified
Cu-ZnO
Electrical conductivity
Catalytic activity
Sol gel

ABSTRACT

Surface modified Cu-ZnO nanostructures with different ratios of Cu (0.0 %, 2.5 %, 5.0 %, 7.5 % and 10.0 %) have been fabricated using a simplified sol gel auto combustion method (SGAC). The utilization of aqueous methanolic solution (50:50 ratio) as the reaction medium, with zinc chloride, ZnCl2, serving as a precursor to modified Cu-ZnO nanostructures and ZnO nanostructures (NSs) in particular, was a novel aspect of this study. XRD, FTIR, SEM, EDX, and UV–Visible spectrum analyses were carried out for the analysis of products. The prepared materials were used to study the electrochemical and photocatalytic properties. By introducing Cu metal on the surface of ZnO, the electrical conductivity was increased, and this attribute was investigated using energy band gap calculations and CV analysis. The energy band gap of fabricated nanostructures found to be decreased from 3.36 to 3.20 eV. The Cu modified ZnO based electrode showed the enhanced relative electron transport and increased peak current which made it to be more efficient in electrochemical applications. Degradation study of Tartrazine azo dye (organic) was carried out to examine the photo-induced catalytic activities of prepared materials under solar radiations, UV-light and darkness. The photocatalytic activity was revealed to be optimum up to 86.12 % when exposed to solar radiations and also with increasing Cu concentration up to 10.0 % on the ZnO surface. When compared to pure ZnO, all synthesized Cu modified ZnO NSs exhibited increased peak current, enhanced relative electron transport and optimized photo-induced catalytic degradation of organic pollutant dye. It was revealed that products manufactured using the SGAC technique had higher quality and produced better results for the intended applications than those previously reported.

1. Introduction

ZnO nanostructures have recently drawn a lot of attention due to their fascinating mechanical, optical, catalytic, and electrical properties [1]. Due to the benefits offered in terms of new reaction mechanisms that are not possible with bulk materials, better volume expansion buffering, and electron transport, a number of researchers are particularly interested in the development of nanostructures to be used as catalyst in waste treatment [2] and also to be used as electrodes for energy related applications [3].

ZnO nanostructures (NSs) are desirable for their emission propensity in blue/ultraviolet and full color lighting because they have a direct wide band gap and comparatively high excitonic binding energy, as well as many radioactive deep level defects [4]. Since ZnO NSs is accidentally n-type, another p-type material is needed to use these properties in LEDs applications [5]. As all p-type polymers have unique properties such as low cost, low power consumption, flexibility, and ease of use. Polymers are a safer option for combining with ZnO NSs to fabricate a lightweight device that takes advantage of both materials' properties for large-area lighting and display applications [6].

To improve their electrochemical behavior and photo-induced hetero-catalytic characteristics, composite surfaces have been intensively

https://doi.org/10.1016/j.inoche.2023.111276
Received 14 March 2023; Received in revised form 8 July 2023; Accepted 20 August 2023
Available online 22 August 2023

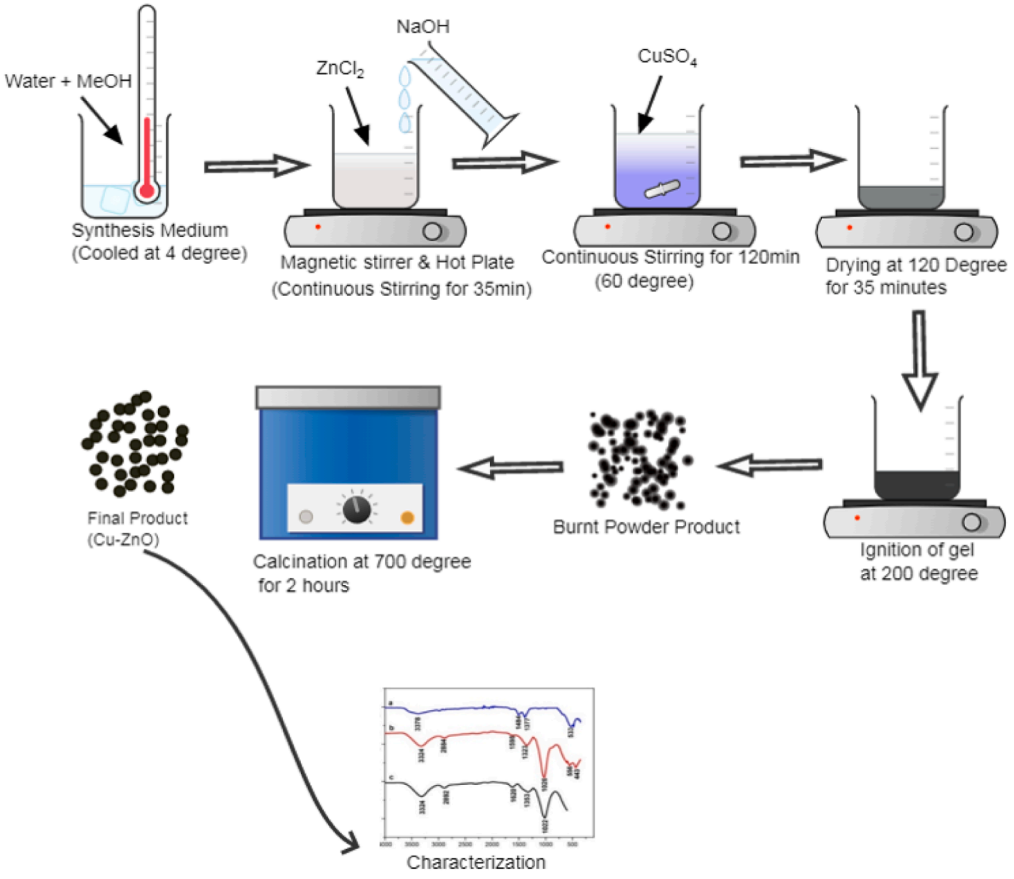

Fig. 1. Synthesis of Surface Modified Cu-ZnO NSs by SGAC.

investigated [7,8]. It is possible to accomplish a number of goals by altering the ZnO nanostructures' surfaces, including strengthening the stability and selectivity of the structures as well as charge transfer kinetics and surface area accessible for catalysis. This has led to the investigation of several surface modification methods and materials.

The deposition of metal or metal oxide nanoparticles onto the ZnO nanostructures is a typical method for surface modification [9]. These nanoparticles have the potential to function as catalytic sites, encouraging certain electrochemical reactions or aiding photo-induced heterocatalytic processes. To increase the catalytic activity of ZnO for particular processes, for instance, noble metal nanoparticles like gold (Au) or platinum (Pt) can be placed on the surface of the material. Improved electrochemical performance results from the presence of extra active sites provided by the metal nanoparticles for the adsorption and activation of reactant molecules [10].

Tuning the energy gap of ZnO NSs has piqued researchers' interest in recent years due to improvements in their properties as well as advancements in efficiency [3]. This improvement is due to the fine-tuning of its energy band gap (EBG) by changing the crystal surface with a variety of transition metals (TM) such as Fe, Co, Ni, Cu, Cd, Hf, and Ag, as well as post-transition metals (TM) such as Bi, Pb, and Al, among others. Among these materials, copper (Cu) is a superior alternative for reducing the EBG of ZnO. By suitably adjusting the stoichiometry ratio of the Cu content, we may minimise the EBG of ZnO NSs and get a novel material with distinct characteristics than their intrinsic counterpart. Hence nano-sized Cu modified ZnO NSs have drawn a great attention in this regard [11].

Doping ZnO nanostructures with foreign elements also has the ability to change their surface characteristics, improve their electrochemical behavior [9], and increase their catalytic activity [12]. Adding more energy levels to the band structure of ZnO by doping with transition metals or nonmetals can result in better charge separation and transfer [6]. The photocatalytic effectiveness of ZnO nanostructures may be improved by this modification, making them more useful in processes including water splitting, pollutant degradation, and solar energy conversion [9].

This research study focused primarily on the synthesis of Cu-modified ZnO NSs by sol gel auto combustion approach, and to use them to optimize their catalytic & electrical properties by decreasing their energy band gap. The aim of this study was to design Cu doped ZnO nanomaterial with tuned energy band gap. The surface modified nanostructured material was then investigated for catalysis against organic dye tartrazine, which has numerous usage in the pharmaceutical and food industrial sectors, yet affects the water quality. Tartrazine's lethal dose in humans is estimated to be 7.5 mg/kg, hence removal is recommended [13].

Sol-gel auto-combustion was the approach employed in a previous study [9] to fabricate Cu-doped ZnO nanoparticles. The researchers looked at how different doping levels affected the structural and optical characteristics. The samples were examined using a variety of characterization methods, including scanning electron microscopy, UV–Vis spectroscopy, and X-ray diffraction [14].

Another study reported the synthesis and characterization of Cu-doped ZnO nanoparticles via the sol–gel auto-combustion approach [15]. The workers studied the influence of the doping concentration on the crystalline structure, particle size, and optical properties of the nano structures. X-ray diffraction, transmission electron microscopy, and photoluminescence spectroscopy were employed to characterize the samples.

Using the sol–gel auto-combustion process, another research team concentrated on the magnetic characteristics of Cu-doped ZnO nanoparticles [11]. The impact of Cu doping on the structural,

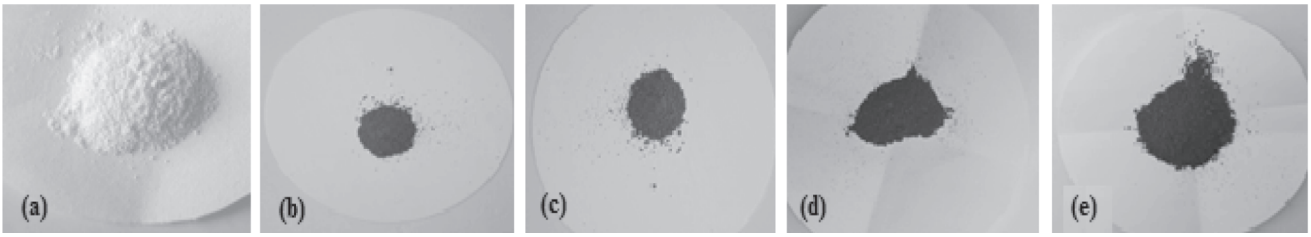

Fig. 2. Cu_X-ZnO; (a) $X = 0.0$ %, (b) $X = 2.5$ %, (c) $X = 5.0$ %, (d) $X = 7.5$ %, (e) $X = 10.0$ %.

morphological, and magnetic characteristics of the nanoparticles is examined by the authors. In order to characterize the samples, methods including electron paramagnetic resonance spectroscopy and vibrating sample magnetometry were applied [16].

2. Materials & methods

Chemicals used in this research were of AR grade; $ZnCl_2$ (Merck Chemicals GmbH, Germany), $CuSO_4{\cdot}5H_2O$ (Riedel-de-Haen Honeywell Chemicals Germany), Methanol (Fischer Chemicals Switzerland), Sodium Hydroxide (Fischer Chemicals Switzerland), and Deionized H_2O.

By using the SGAC Approach, ZnO and surface-modified Cu(x)-ZnO ($x = 0.0$ %, 2.5 %, 5.0 %, 7.5 %, and 10.0 %) NSs were synthesized (Fig. 1). For synthesis, AR chemicals and reagents were employed. A 50:50 mixture of MeOH and distilled water was employed as a solvent system to prepare the reaction medium. According to the stoichiometric ratio, (1:2) of $CuSO_4{\cdot}5H_2O$ to NaOH; the oxidizer and $ZnCl_2$ was selected and dissolved in a small amount of solvent in a typical synthesis of Cu_x-ZnO samples. To obtain a homogenous solution, the combined solution

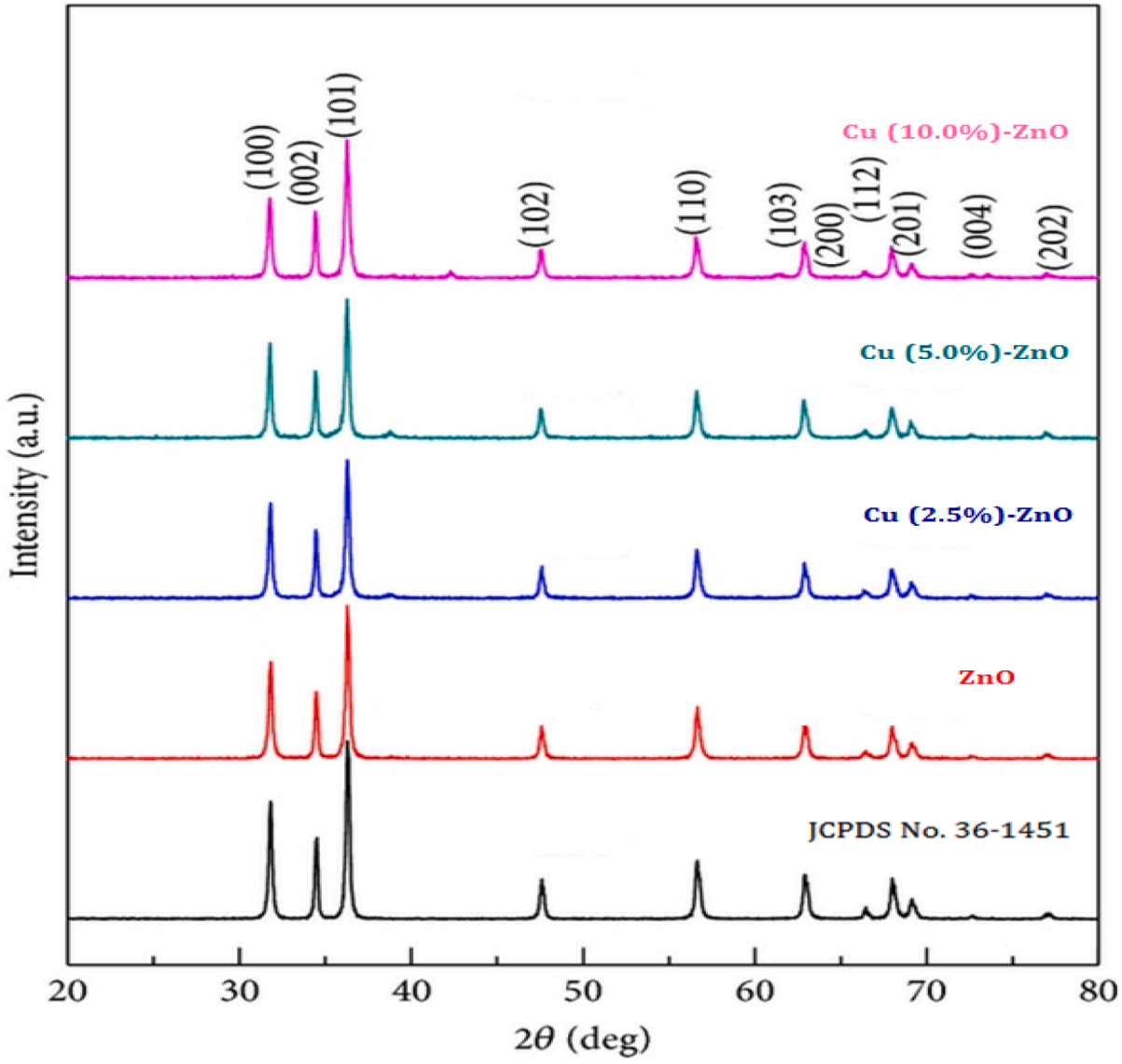

Fig. 3. XRD Patterns of Synthesized Products.

was continuously stirred for two hours followed by heating up to 120 °C with stirring, resulting in the production of viscous gel. By increasing the temperature up to 200 °C, this gel was burned, and after remaining for a while, burnt powder material was obtained. The burned material was then calcined at 700 °C for two hours to produce modified Cu-ZnO NSs and ZnO. The finished products were analyzed for analytical characterization. Schematic representation is given in Fig. 1.

2.1. Characterization of prepared nanostructures

The synthesized NSs were thoroughly examined using a variety of analytical approaches. Nova NanoSEM 450 field-emission scanning electron microscope (FE-SEM) was used to explore the surface morphologies. By employing Cu-K (λ = 1.54178 Å) in the range of 20–60° at Bruker D8 Advance XRD instrument, the crystallinity and crystal phases of the produced NSs were examined. The chemical structures and functional groups were identified using Compact FT-IR spectrometer Alpha-II by Bruker, Germany in the range of 450–4000 cm^{-1}, and the chemical compositions were evaluated using EDX coupled with FE-SEM.

Varian Cary 100 UV–VIS Spectrophotometer was used to investigate the optical properties in the 200–800 nm region at room temperature. Using EDX Analysis to determine the elemental compositions, it was possible to examine the effects of Cu additions on the structure of ZnO crystals. In order to ascertain the EC of synthesized NSs, the results of UV–Visible Spectroscopy were used to calculate the EBG. Electrochemical studies were done by cyclic voltammetry analysis. Varian Cary 100 UV–VIS Spectrophotometer was used to research the photo-catalytic degradation of organic dye utilizing ZnO and modified Cu-ZnO NSs as the photocatalyst.

2.2. Electrochemical studies by energy band gap & cyclic voltammetry

To study electrochemical behavior, the energy band gap (EBG) of prepared samples, the UV–Visible spectrophotometer was used and absorption was recorded. Later, by applying the energy equation, EBG was calculated.

By using cyclic voltammetry (CV), electrochemical experiments were conducted. At sweep rates of 100 mVs^{-1}, CV in the −0.5 to 0.5 V voltage range were observed. A working electrode consisting of an Au disc coated with ZnO and Cu-ZnO NSs was used to perform the experiments in 0.1 M NaCl solution. Ag/AgCl was employed as the reference electrode in the tests, while a Pt wire served as the counter electrode. Following the thin film's coating by dripping aqueous ZnO and Cu-ZnO solutions onto an Au disc with a 2.0 mm diameter.

2.3. Dye degradation by photo-induced hetero catalysis

To investigate the photo-induced heterocatalytic properties of prepared samples, the Tartrazine azo group dye was used to degrade under different conditions. The reaction setup was run for 120 min and after every 10 min, the minimum amount of sample was collected and analyzed for the kinetic analysis of dye degradation processes.

UV–Visible spectra and absorbance at 426 nm were recorded. The amount of dye in each sample was calculated using UV–visible spectroscopy. All studies were conducted with dye solutions at their normal pH and then at pH 6.0. %Degradation of dye was determined using the Equation (% Degradation = $[(A_o - A_t)/A_o] \times 100 = (C_o - C_t/C_t) \times 100$), Where, A_o is absorbance of dye at initial stage, A_t is absorbance of dye at time "t", C_o is initial concentration of dye before irradiation and C is concentration of dye after irradiation.

3. Results and discussions

The SGAC approach was applied to fabricated the pure ZnO and modified Cu-ZnO (Cu = 2.5 %, 5.0 %, 7.5 %, & 10.0 %) NSs. The main factors of using methanolic solution as reaction solvent were solubility of used salts, reaction kinetics of this fabrication process, control of surface modifier distribution and environmental safety. The color and product texture were examined to assess the physical appearance (Fig. 2a–e). Off white color with fine texture represented the formation of ZnO NSs while blackish colored granular powder confirmed the formation of Cu modified ZnO NSs.

Table 1
XRD Results of Pure ZnO & Cu modified ZnO NSs.

Sr	Product Name	Cu-Kà (Å)	Unit Cell values	Calculated Density (g/cm^3)	DOC	Average Crystallite Size (nm)
1	ZnO	1.541874	a = 3.2493 c = 5.2057 I/IC = 6.77	5.678	96.9 %	33.8
2	Cu_x-ZnO (x = 2.5 %)	1.541874	a = 3.2493 c = 5.2071 I/IC = 7.16	5.568	94.8 %	103.2
3	Cu_x-ZnO (x = 5.0 %)	1.541874	a = 3.2490 c = 5.2061 I/IC = 6.88	5.682	95.6 %	143.5
4	Cu_x-ZnO (x = 10.0 %)	1.541874	a = 3.2492 c = 5.2072 I/IC = 7.16	5.569	92.8 %	174.9

3.1. XRD analysis

XRD examination was carried out to evaluate the crystallinity and crystal phase of produced ZnO NSs and modified Cu-ZnO NSs. The results are shown in Fig. 3. It is possible to see well-defined diffraction reflections that strongly resemble the hexagonal phase of pure wurtzite. With a monochromatic Cu-K radiation source at λ = 1.5406 A°, the Bruker D8 Advance XRD equipment was utilised to analyse all of the fabricated NSs in the diffraction angle range of 20°-60°.

Table 1 listed the computed average crystallite size, lattice parameters, and crystal phase evaluated by the Scherrer formula. These results supported the hexagonal organisation and nanoscale size of the produced NSs. When these results are compared to JCPDS data, it is discovered that they are comparable to the XRD pattern of ZnO found on JCPDS Card No.: 36-1451. These findings further showed that the hexagonal structure of ZnO was not altered by the addition of Cu metal [17]. By using XRD analysis, the degree of crystallinity (DOC) was also studied to evaluate if addition of Cu metal affected the crystal structure. It was observed that the DOC was only marginally dropped from 96 to 92 %, which is insignificant, while the Cu content increased from 0.0 % to 10.0 % (Table 1).

3.2. Functional group analysis

The chemical compositions, functional group analysis, and quality of fabricated pure ZnO and modified Cu-ZnO NSs were investigated at room temperature using FT-IR Spectrophotometer. All of the fabricated samples were evaluated under identical parameters and conditions. Different definite peaks at 545–570 cm^{-1}, 1415–1440 cm^{-1}, 1455–1470 cm^{-1} and 3415–3470 cm^{-1} have been observed in FTIR analysis (Fig. 4). The sharp peak in range of 545–570 cm^{-1} confirmed the fabrication of ZnO lattice. The sharp peak in the range of 1415–1440

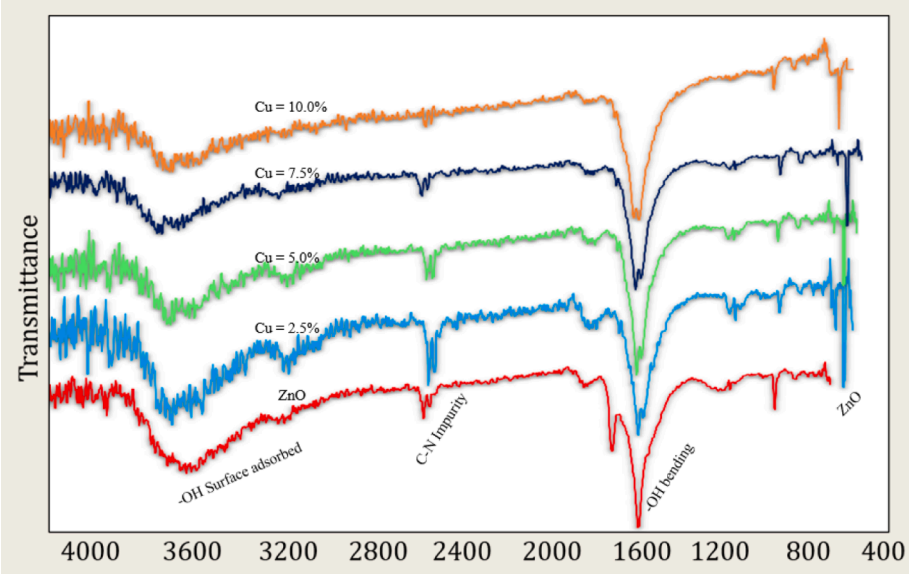

Fig. 4. Functional Group Spectra of Synthesized Products.

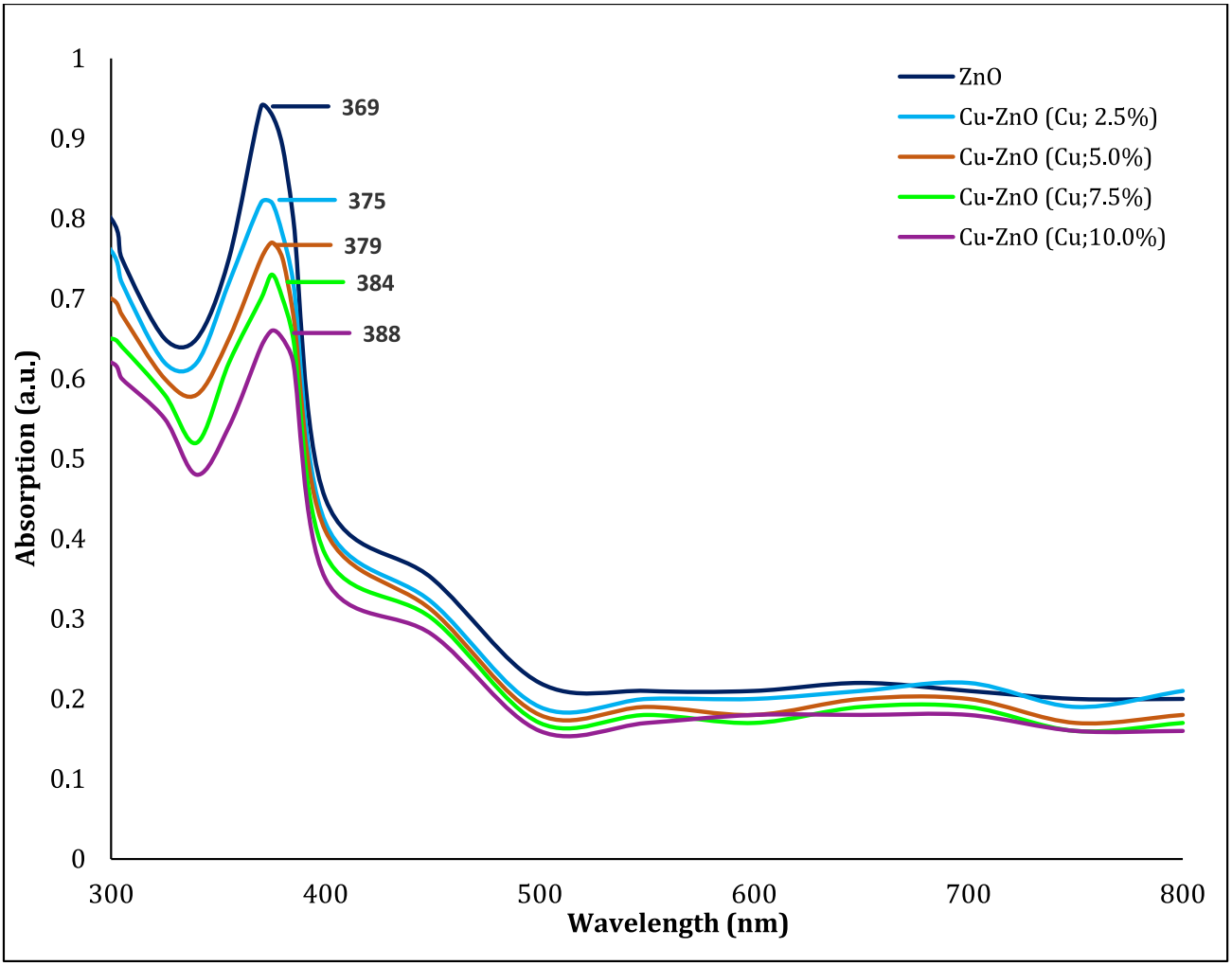

Fig. 5. UV–Visible spectra of prepared products.

Table 2
UV–Visible Spectroscopic Results of Pure ZnO & modified Cu-ZnO NSs.

Sr.	Product	λ_{max} (nm)
1	Pure ZnO	369
2	Cu_x-ZnO (x = 2.5 %)	375
3	Cu_x-ZnO (x = 5.0 %)	379
4	Cu_x-ZnO (x = 7.5 %	384
5	Cu_x-ZnO (x = 10.0 %)	388

cm^{-1} confirmed the hydroxyl group due to use of H_2O in fabrication. The signal in range of 1455–1470 cm^{-1} confirmed presence of methyl group which may come from methanol used in fabrication. The broad signal in range of 3415–3470 cm^{-1} represented the O—H stretching due to surface adsorbed water content (H—OH) [1]. An impurity with C—N functionality was detected due to the signal in range of 2340–2380 cm^{-1} which may be due to surrounding environment of products [18].

3.3. UV–Visible spectroscopic analysis

Modified Cu-ZnO NSs and ZnO were studied through UV–visible (UV–Vis) spectroscopic analysis for energy band gap calculation and catalytic behavior. Homogeneous dispersion of the nanomaterials was prepared in DMSO under ultrasonication for 1 h. Fig. 5 represented the normal UV–Visible spectra of pure ZnO and modified Cu-ZnO NSs, and distinct absorption peaks in the region of 369–388 nm were observed (Table 2). Red shift was observed with the doping of Cu metal. As the Cu concentration increased from 0.0 % to 10.0 %, the wavelength with maximum absorption was shifted from 369 nm to 388 nm (Fig. 6). This red shift reflected a change in the optical characteristics of ZnO NSs and might favor an alteration in EBG, thus facilitating the absorption of radiation which favors the photocatalytic activity of the nanomaterial.

3.4. SEM analysis

Scanning electron microscopy was carried out to examine the crystal surface morphologies of the produced samples. Fig. 7 displays the SEM micrographs of pure ZnO and modified Cu-ZnO NSs. These micrographs showed that with the increased contents of Cu, the morphology and form of produced ZnO NSs was slightly affected. The effects of Cu contents on the homogeneity and shape of synthesised ZnO NSs are also consistent with the results of *Saad et al.* (samples with Cu 1.0 % to 3.0 % using co precipitation method), who hypothesised that this could be because more Cu ions are being substituted with Zn sites [19].

The synthesised NSs were displayed with reasonably uniform size distributions and somewhat greater size in the SEM image for ZnO (Fig. 7-a). This might be proof that the first NSs phase was aggregated to grow the second NSs phase. With increasing Cu contents, NSs appear to become more agglomerated in Cu-ZnO NSs, making it impossible to determine anything about typical grain sizes from these less-resolved SEM micrographs (Fig. 4 b–e).

3.5. EDX analysis

To evaluate the elemental composition of produced ZnO NSs and the presence of Cu contents on ZnO NSs, the EDX analysis was carried out. Here, a chemical micro-analysis method called EDX was combined with a scanning electron microscope.

Figs. 8 and 9 showed the actual EDX images of the fabricated ZnO NSs and Cu-ZnO NSs (with Cu: 5.0 %), respectively. Table 3 reports the elemental composition of samples created using SGAC technique. EDX graphs of fabricated NSs showed that Cu content in fabricated NSs is quite similar to the nominal levels. Zn, Cu, O, and C make up these NSs. The presence of C on the surface of the NSs, which was also confirmed by FTIR analysis, was the cause of the C impurity that was visible in the products produced using this method.

3.6. Energy band gap study of ZnO and Cu-ZnO NSs

The optical energy band gap (EBG) of fabricated pure ZnO and Cu modified ZnO NSs were calculated using photon energy equation ($E_g = hc/\lambda$), Where h, c are the constants while λ is the wavelength value at which well-defined peak appeared. E_g is the calculated value of Optical EBG. In pure ZnO NPs, top of valence band (VB) and bottom of the conduction band (CB) are at higher symmetrical level, while top of VB is at zero energy level (E_g = 0), suggesting the pure ZnO NPs. EBG of synthesized ZnO NPs in this study was calculated as 3.36 eV which is closest to its theoretical value (3.37ev). The EBG decreased when Cu was introduced to the ZnO lattice. EBG continues progressively declining as Cu-metal concentration rises. This quality gives the photo-anodes based on solar cells and ZnO anodes in Li-ion batteries the enormous scope and opportunities to achieve better absorption in the visible ranges [20].

The mechanism of band gap tuning may be proposed based on the electronic configuration of the ions during the following ionic reactions which was expected to be occurred.

$$ZnCl_2 + 2NaOH \xrightarrow{CH_3OH + H_2O} Zn\text{ - }O + 2NaCl\ (ppt)$$

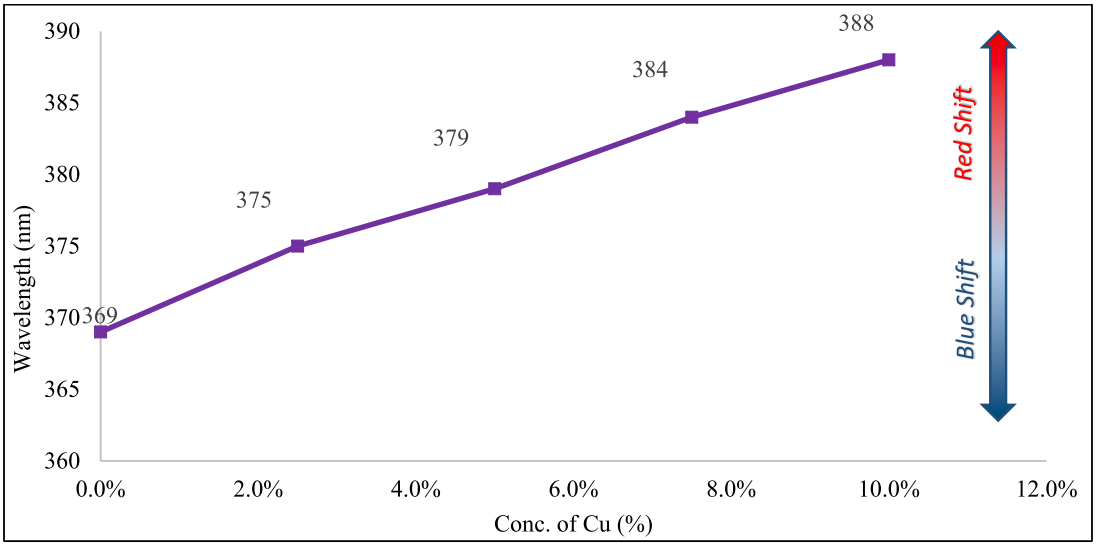

Fig. 6. Effect of Cu content on Wavelength for ZnO & Cu-ZnO NSs.

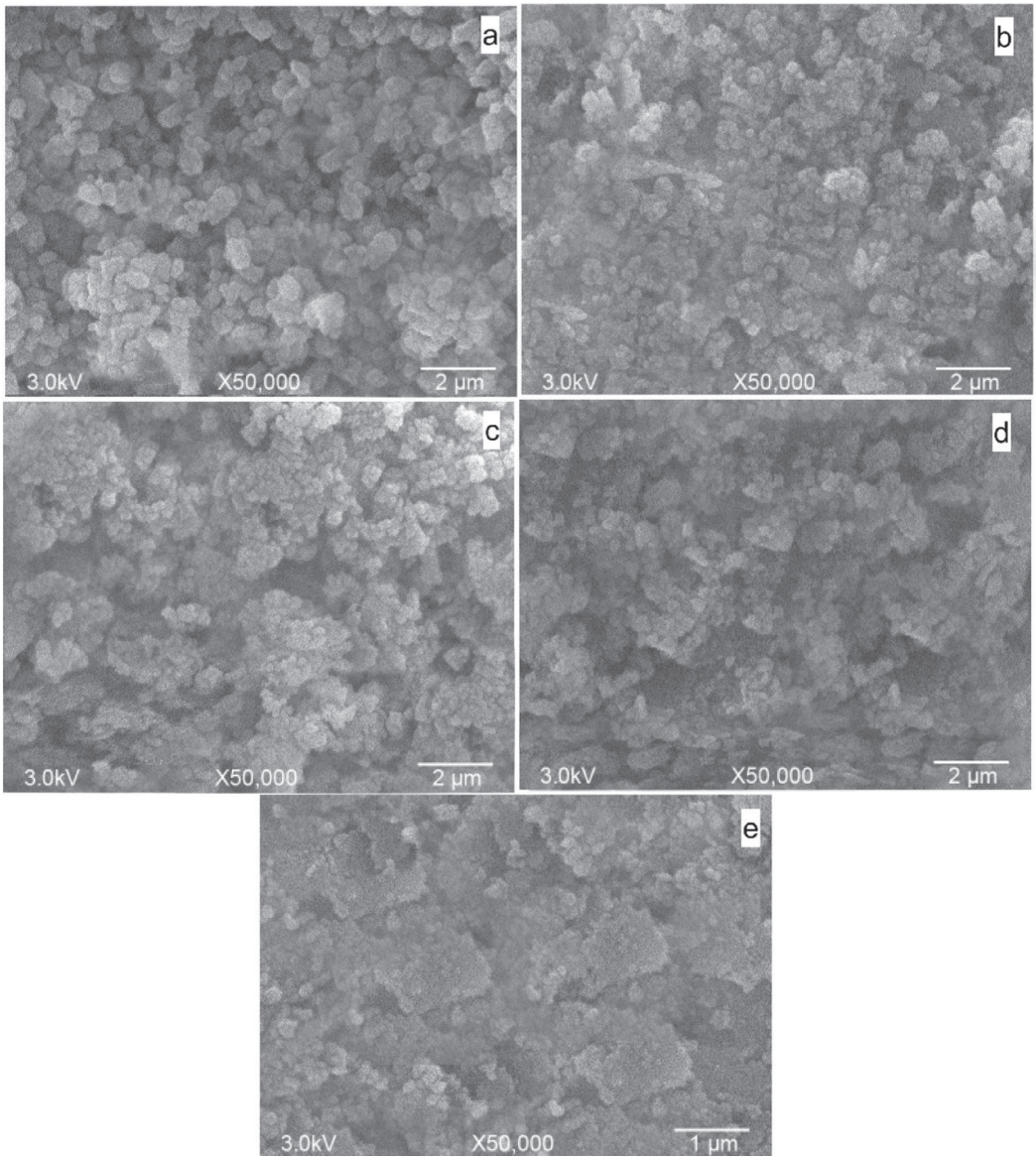

Fig. 7. SEM images of (a) ZnO (b) 2.5 wt% (c) 5.0 wt% (d) 7.5 wt% (e) 10 wt% Cu- ZnO NSs.

$$ZnCl_2 + CuSO_4{\cdot}5H_2O \xrightarrow[NaOH]{CH_3OH + H_2O} Cu\text{ - }Zn\text{ - }O + 2NaCl\ (ppt)\ +\ H_2SO_4(g)$$

When Cu^{+2} is added, the 3d and p electrons (of cu or Zn???) exhibit a repulsive behavior that raises the CB energy and decreases electrical conductivity while increasing EBG. However, when the Cu-metal concentration raised, the amount of Zn-3d electrons in the VB dropped, which lessened the p-d rejection impact at the top of the VB. Increases in Cu concentration result in increases in the concentration of Cu-3d and Cu-3p electrons while remaining constant in the concentration of O-2p electrons, which also helped to optimize the d-p repulsion effect at the top of VB [21].

The increased Cu content and changed EBG optimise this phenomena. The inclusion of Cu^{+2} ions allows the electrons on top of VB to shift lower, resulting in a very tiny electron-binding group (EBG), which improves the passage of electrons between VB and CB, potentially increasing the electrical conductivity of Zn NSs [22].

Using equation ($E_g = hc/\lambda$), the EBG of produced ZnO/Cu doped ZnO NSs was determined. Table 4 lists the computed values and absorption wavelength for each sample. These computed and actual figures showed that the EBG was high and the conduction character was low when no additional metal was added to the structure of ZnO NSs, which is why pure ZnO behaved as a semiconductor. However, when the Cu metal was included into the ZnO NSs structure [23], it may have filled the oxygen vacancies in the structure, and as a result, the EBG was lowered from 3.36 eV to 3.20 eV (Table 4). As the Cu contents increased, the EBG value decreased as well (Fig. 10). And from the research studies, it is proven that lower the EBG value, higher will be EC of ZnO NSs [24].

Due of the oxygen vacancies it contains, ZnO is an n-type semiconductor on the surface, but due to its high EBG of 3.36 eV, it is exclusively UV light active (or 3.37 eV). Thus, instead of simply being UV light active, ZnO becomes visible light active when the optical EBG drops. As a result, the CB and VB of ZnO produce more electrons and holes, respectively. Doping, generating heterojunctions, and introducing defects are frequently employed to increase the EC of ZnO crystal lattices. When a result, as the EBG narrows, the electrical conductivity (EC) of ZnO will rise [25]. The EBG reduces when Cu metal is added to the ZnO NS structure, and the Cu metal concentration increases. ZnO NSs may diminish as the concentration of Cu metal in the structure increases incrementally [26]. The EC of ZnO NSs may be enhanced due to a decrease in EBG of ZnO NSs caused by the considerable rise in Cu metal content in ZnO NSs structure [27].

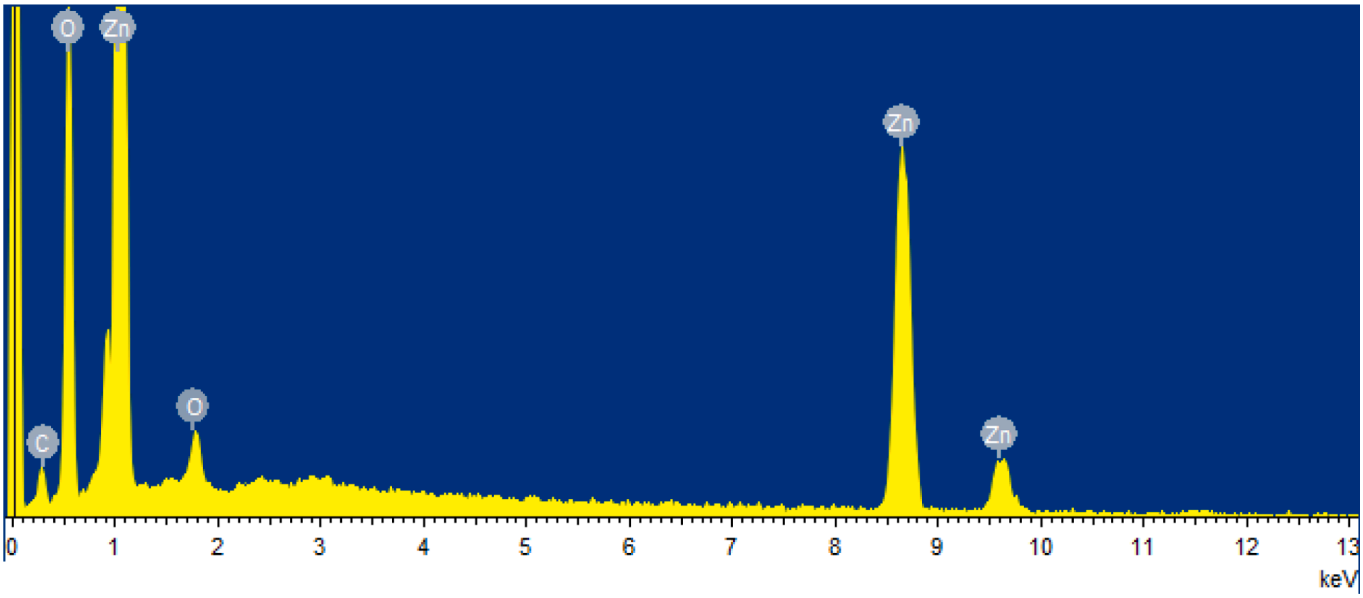

Fig. 8. EDX Image of ZnO.

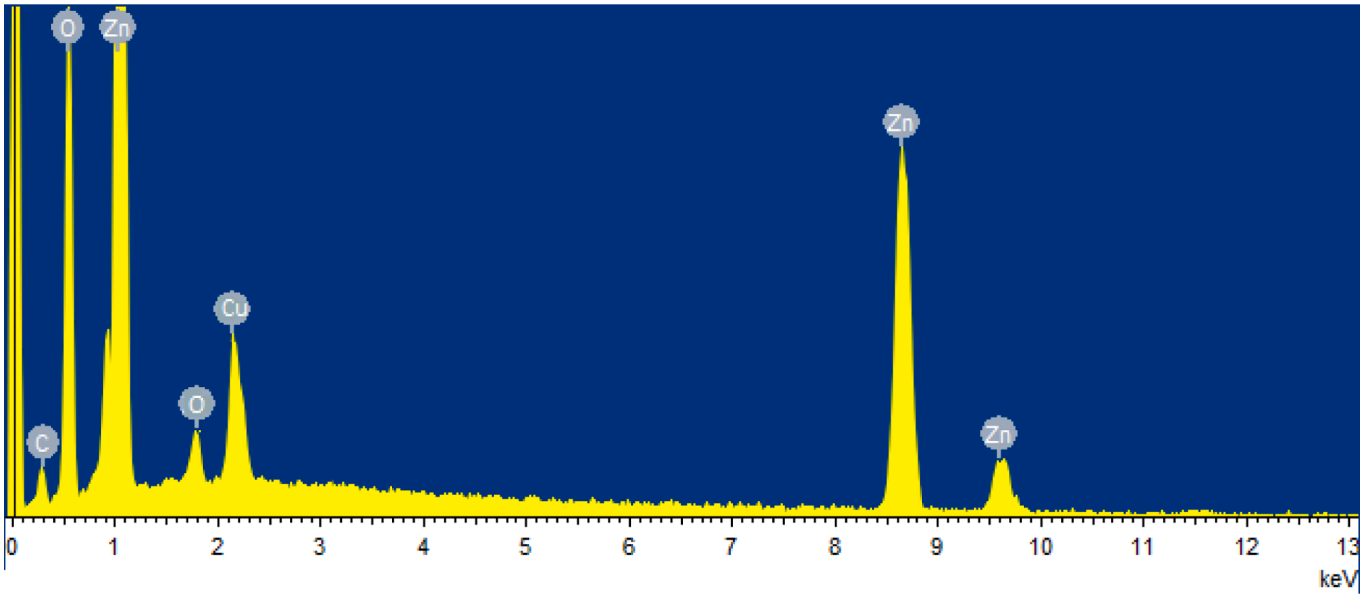

Fig. 9. EDX Image of Cu-ZnO NSs (Cu 5 % wt).

Table 3
EDX results of Synthesized NSs.

No.	Product	Element Compositions (Detected)
3	ZnO	Zn = 48.67 % O = 47.31 % C = 4.02 %
4	Cu_x-ZnO (x = 5.0 %)	Zn = 47.31 % O = 44.87 % Cu = 4.87 % C = 2.95 %

Table 4
Calculated EBG and Absorption Maxima of ZnO/Cu doped ZnO NSs.

Sr.	Product	Absorption Wavelength (nm)	EBG (E_g)
1	ZnO	369	3.36
2	Cu-ZnO (*Cu* = 2.5 %) NSs	374	3.31
3	Cu-ZnO (*Cu* = 5.0 %) NSs	378	3.27
4	Cu-ZnO (*Cu* = 7.5 %) NSs	382	3.23
5	Cu-ZnO (*Cu* = 10.0 %) NSs	387	3.20

3.7. Electrochemical studies

In 0.1 M NaCl aqueous solution, CV analysis was conducted at a scan rate of 100 mV/s in potential range of +0.5 to −0.5 V. Fig. 11 displays the CVs of pure ZnO, Cu-ZnO nanostructure thin films at 2.5 %, 5.0 %, and 10.0 %. The distinct redox peaks at the pure ZnO thin film CV curve have not been found. Two peaks showing the oxidation were appeared at 0.252 V and −0.122 V in the 2.5 % Cu-ZnO nanostructure thin film's behavior in terms of cyclic voltammetry, as well as two peaks at −0.316 V and 0.214 V which showed the reduction. Two oxidation peaks at

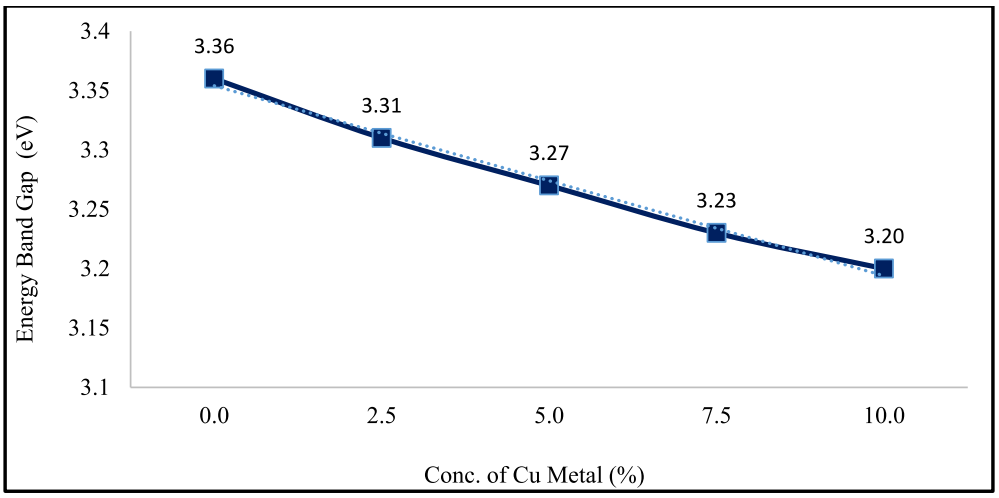

Fig. 10. EBG Decreasing Trend of ZnO & Cu-ZnO NSs.

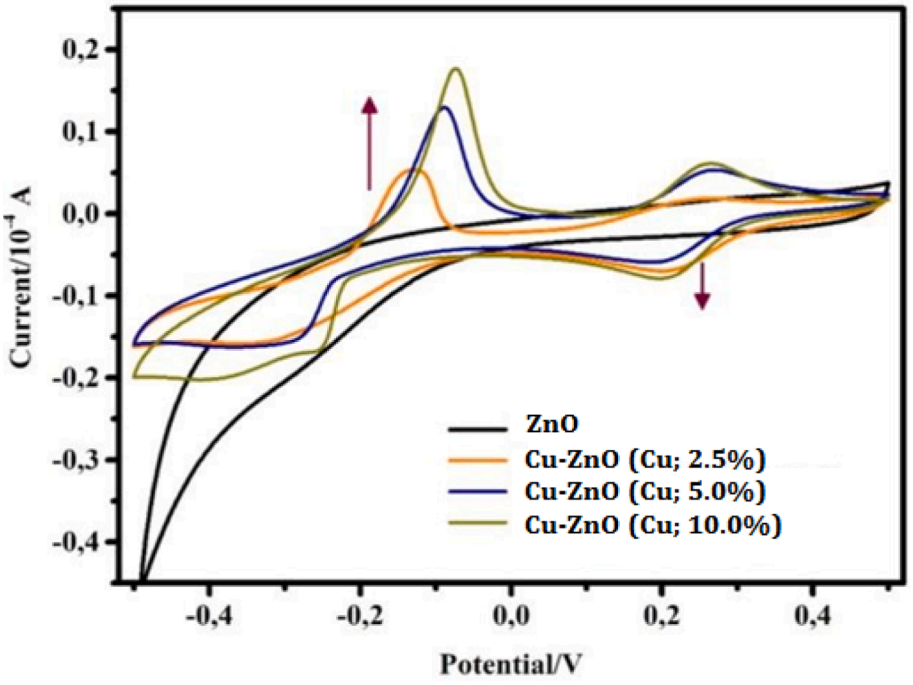

Fig. 11. CV curves of ZnO, 2.5 %, 5 % and 10 % Cu-ZnO NSs at a scan rate of 100 mV/s in 0.1 M NaCl aqueous solution.

0.262 V and −0.086 V, as well as two reduction peaks at −0.318 V and 0.214 V, were seen in a 5.0 % Cu-ZnO nanostructure thin film. Two oxidation peaks at 0.266 V and −0.066 V, as well as two reduction peaks at −0.342 V and 0.204 V, were seen in a 10 % Cu-ZnO nanostructure thin film. Voltamogram results show that the addition of Cu prevents oxidation as the first oxidation peaks shift toward a more positive potential. The CV loops of ZnO & Cu-ZnO NSs have been shown that the electrode surface experiences better charge dissipation. It was discovered that Cu-modified ZnOs outperformed pure ZnO in terms of electrochemical characteristics [28]. This demonstrates how adding Cu to ZnO thin films may enhance relative electron transport [1]. When compared to pure ZnO, all manufactured Cu modified NSs exhibit increased peak current. The Cu modified electrode may thus be more advantageous in electrochemical applications, according to this [29]. Peak current has increased in virtually all samples as the concentration of Cu content has increased.

3.8. Degradation of organic pollutant dye by photo induced hetero catalysis

The second goal of this research was to study the efficiency of photo induced catalytic degradation of tartrazine dye (TD), an organic azo group employing ZnO/Cu doped ZnO Nano structures as photo catalysts and UV light, solar radiations, and darkness as irradiation sources. In this study, the yellow TD solution was treated with fabricated NSs that were employed as a photocatalyst under irradiation sources, and the color of the solution was discharged (Fig. 12). This investigation was also done to compare the photocatalytic degradation (%) of TD under different conditions such as quantity of Cu metal, exposure period, pH of dye solution, availability and unavailability of irradiation sources and photo catalyst. A UV–Vis spectrophotometer was used to study the photodegradation of TD.

The results demonstrated that the degradation of TD employing ZnO as a photocatalyst was successful in the presence of sun light. The best

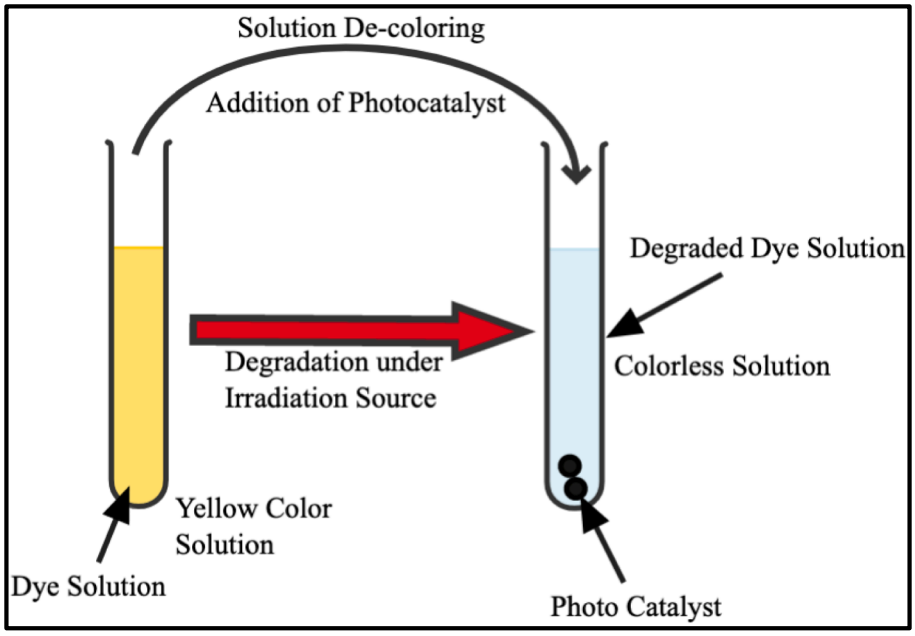

Fig. 12. Discoloration of colored dye solution.

Table 5
Photocatalytic degradation (%) of TD.

Sr.	Product Name	Solar radiations		UV-Light		Darkness	
		% *D*	R^2	% *D*	R^2	% *D*	R^2
1	ZnO	32.15	0.9917	34.16	0.9333	29.55	0.9515
2	Cu-ZnO (*Cu* = 2.5 %)	46.51	0.9871	42.61	0.9578	35.66	0.9886
3	Cu-ZnO (*Cu* = 5.0 %)	57.54	0.9925	55.61	0.9786	42.69	0.9923
4	Cu-ZnO (*Cu* = 7.5 %)	69.74	0.9987	65.19	0.9918	45.15	0.9949
5	Cu-ZnO (*Cu* = 10.0 %)	86.12	0.9838	72.16	0.9748	48.98	0.9921

*%D = % degradation.

Table 6
Degradation (%) of TD by ZnO & Cu-ZnO NSs under Solar radiations at optimum pH 6.0.

Sr.	Product	% Degradation
1	ZnO	30.22
2	Cu-ZnO (*Cu* = 2.5 %)	45.58
3	Cu-ZnO (*Cu* = 5.0 %)	60.58
4	Cu-ZnO (*Cu* = 7.5 %)	85.85
5	Cu-ZnO (*Cu* = 10.0 %)	92.51

degradation occurred at the optimum ZnO weight, pH of dye solution, and radiation exposure duration. The ideal catalyst weight under photocatalytic conditions was 10 mg, when the catalyst demonstrated highest dye degradation.

The best degradation occurred under ideal conditions of Cu-ZnO (Cu = 10.0 %) catalyst, sun radiation, and pH 6.0. 75–10 % of TD had deteriorated after the 120-minute irradiation period.

In order to produce $OH^{\bullet}$, a catalyst and sun radiation were both necessary. ZnO and Cu-doped ZnO NCs were employed as photocatalysts for the degradation of TD under the influence of sun radiation. Using a UV–Visible spectrophotometer (Agilent Carry-100 series), the absorbance was measured to assess the rate of dye degradation. From the absorbance, the concentration of dye was calculated at equal intervals of time. The results on each time point are explained in Tables 5 and 6. The concentration of dye was determined from the initial absorbance (A_o) of the dye and the absorbance (A_t) after irradiation.

Figs. 13 and 14 showed that as irradiation duration increased, dye concentration declined and degradation performance (%) increased. The highest degradation in solar radiations was up to 86.12 % after the entire period (Table 5). Maximum degradation was reported to be up to 72.16 % under UV-254 nm, whereas degradation was up to 48.98 % in the absence of light. Pure ZnO NPs were shown to produce lower outcomes than any other Cu modified ZnO NSs. Additionally, it was shown that the rate of TD degradation steadily increased as the concentration of Cu metal increased proportionally. The dye degradation rate determined by applying the pseudo-first-order kinetics is shown in Figs. 16–18 and their R^2 values are given in Table 5.

3.9. Effect of irradiation time on degradation of TD

With the passage of irradiation time intervals as the interaction time with the irradiation source (solar radiations, UV-254 nm light, and in the absence of an irradiation source) increased, all of the aforementioned results showed that the photocatalytic degradation (%) of TD increased and the dye concentration in the prepared solution decreased (Figs. 13–15).

3.10. Photocatalytic degradation mechanism of TD

While using UV–visible light (UV-254 nm), solar radiations, and darkness as irradiation sources, researchers found that the photocatalytic degradation methods of TD on pure ZnO and Cu modified ZnO NSs differed from one another. The degradation and breakdown of an organic dye's macromolecule into its smaller molecules occurs mostly (Fig. 19).

It is a commonly accepted theory that when solar radiations or UV radiation hit the surface of the photocatalysts, photons stimulated the electrons in VB, causing them to move up to CB. As a result of this irradiation, the electron and the hole pairs (e^- & h^+) are produced (Figs. 20–23). Both will interact with water and oxygen on the surface of the ZnO to generate the oxidizing agents including H_2O_2, $^{\bullet}O_2^-$ and $^{\bullet}OH$, in which $^{\bullet}O_2^-$ and $^{\bullet}OH$ are the strong oxidizing agents. They can degrade the organic compound into H_2O_2 and CO_2. However, the some of the electrons (e^-) lying on the CB is extremely short, the electrons almost

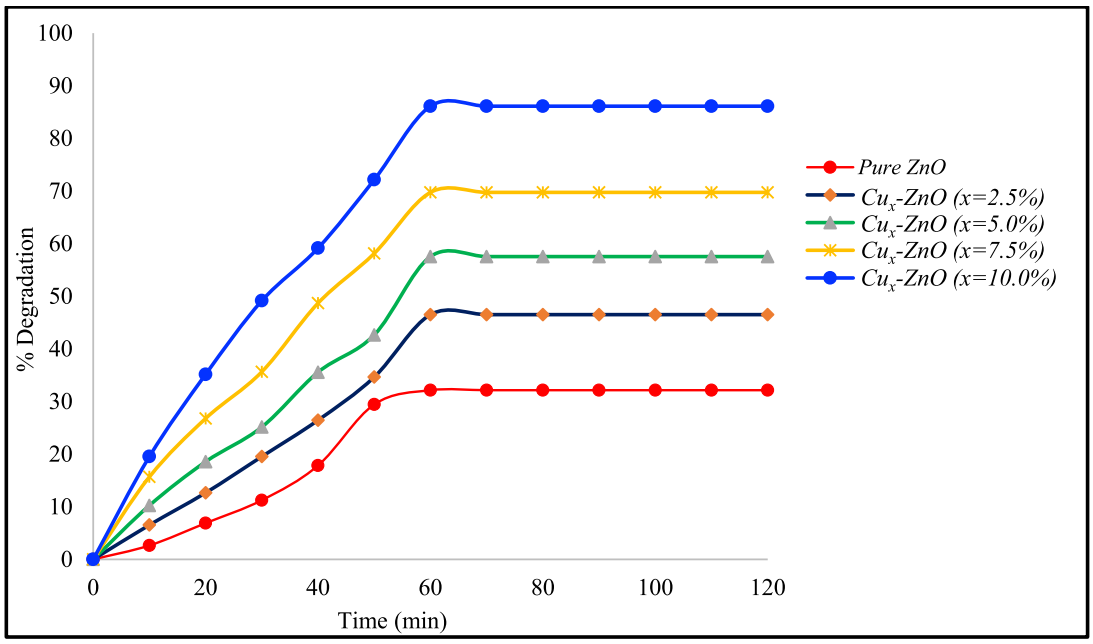

Fig. 13. Degradation of TD under solar radiations.

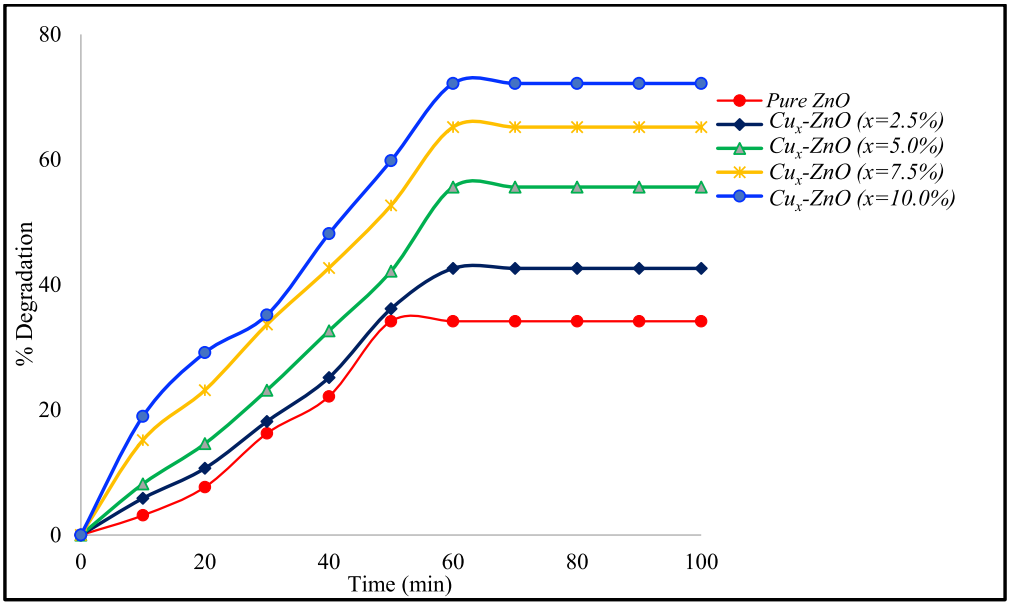

Fig. 14. Degradation of TD under UV-254 nm.

immediately release the energy to return to the ground state to recombine with hole (h^+) originally, and this is one of the most significant limitations of pure ZnO NSs [30].

3.11. *Effect of metal doping on degradation efficiency of ZnO NC's*

When Cu metal is added to the surface of ZnO NSs and these Cu-modified ZnO NCs are utilised as photo catalysts, the "Schottky Barrier" (potential energy barrier for the electrons produced at a metal-ZnO junction) is established between Cu metal and ZnO. This is due to the fact that the energy level of ZnO's CB is greater than the fermi level of Cu-ZnO, allowing free electrons in CB to move from ZnO (Figs. 19–20) [31].

Metal electrons can generate the $\bullet O_2^-$ free radical, whereas holes in the VB may react with H_2O_2 to generate the $^{\bullet}OH$ radical. [32]. These free radicals can degrade the organic compounds to CO_2 and H_2O the mechanism can be explained by;

$$ZnO + h\nu\ (UV) \rightarrow ZnO\ (e^-) + h^+$$
$$ZnO\ (e^-) + Cu \rightarrow ZnO + Cu\ (e^-)$$
$$Cu\ (e^-) + O_2 \rightarrow {}^{\bullet}O_2^- + Cu^{\cdot}$$
$$ZnO\ (h^+) + H_2O \rightarrow ZnO + H^+ + {}^{\bullet}OH$$
$$({}^{\bullet}O_2^- + {}^{\bullet}OH) + Dye \rightarrow Intermediate\ Product$$
$$Intermediate\ Products + Free\ radicals \rightarrow CO_2 + H_2O$$

The findings demonstrated that pure ZnO NSs have less photocatalytic activity than Cu-modified ZnO NSs. The Degradation rose along with the ratio of Cu metal. Due to the fact that under solar radiations and other visible light irradiation, metallic NSs may produce electrons via the surface plasma resonance (SPR) phenomenon, which may lead to

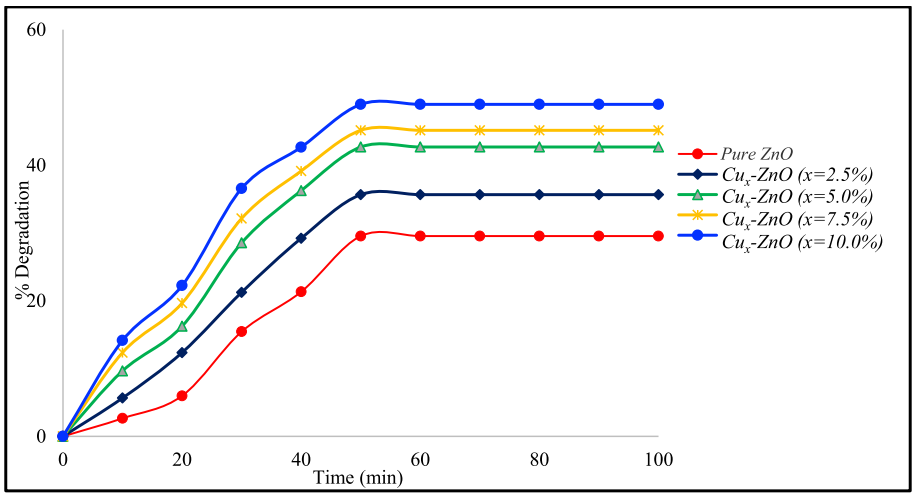

Fig. 15. Degradation of TD in absence of irradiation source.

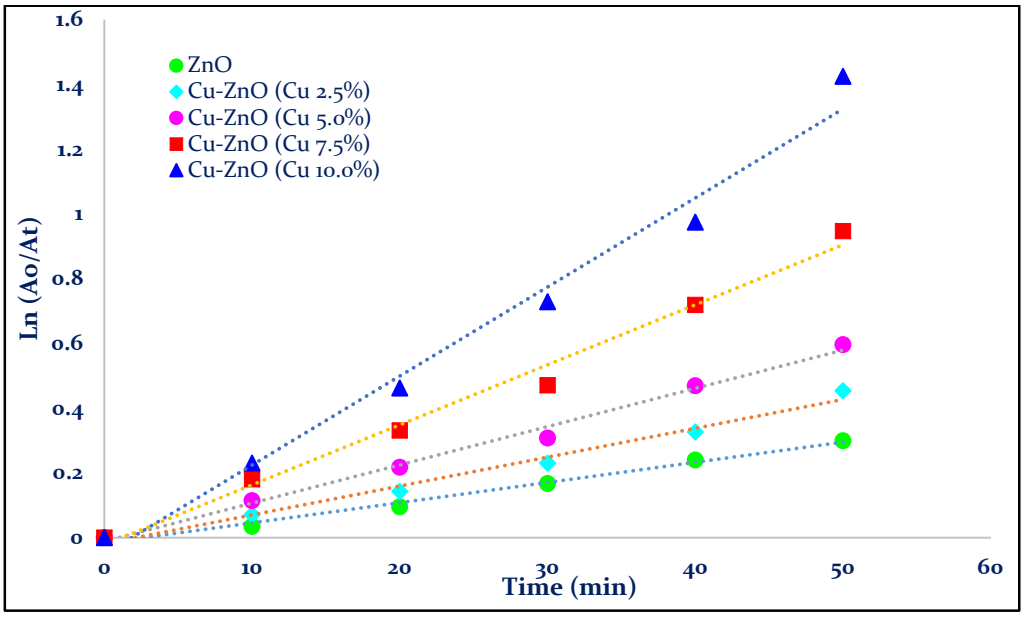

Fig. 16. Pseudo-first order kinetics of dye degradation under sunlight.

high absorption light in the visible range, Cu modified ZnO NSs demonstrated dramatically improved photocatalytic activity. Although it can restrict the flow of electrons from metal to ZnO NSs, the Schottky bsarrier is generated at the metal–semiconductor interface.

Many studies conducted until now have demonstrated that the Cu-ZnO interface's strong electrons, which oscillate collectively on the SPR excitation zone, can allow electrons to pass across the Schottky Barrier. As a result, electrons may transfer from a metal to the CB of ZnO.

The oxygen molecules that have been adsorbed then scavenge them, producing superoxide radical anions ($^{\bullet}O_2^-$) that break down the dye molecule. Meanwhile, the organic contaminants might be directly oxidised on the photocatalyst surface by the photogenerated holes, leading to an enhanced photo-induced catalytic degradation in the visible light range.

3.12. *Effects of dye solution pH on photocatalytic degradation*

In general, a key consideration for well-planned reaction processes is the pH value of dye solutions (and pollutant solutions). It has a significant impact not only on the surface charges and functional groups of adsorbents, but also on the structure, and ionization level of dye molecules. This study observed at how dye degradation is impacted by the pH of the starting solution. At two pH levels between 5.0 and 6.0 under fixed other circumstances, the degrading performance was assessed (dosage catalyst, time, concentration of dye solution). The effectiveness of dye degradation was significantly impacted by pH. The degradation efficiency dramatically increased at an ideal pH of 6.0 when pH increased from 5.0 to 6.0 (Table 6). The pH of the dye solution was elevated by around 6.0 % as compared to the Cu$_x$-ZnO (x = 10.0 %) NSs, which demonstrated about 92.51 % dye degradation. In the presence of a photocatalyst, the pH had a considerable impact on dye degradation.

The optimal pH for dye degradation on ZnO and Cu/ZnO was found to be 6.0. At pH levels lower than 6.0, degradation efficiency is limited; nonetheless, the degradation ended owing to ZnO dissolution in an acidic media, as shown below.

$$ZnO_{(s)} + 2H^+_{(aq)} \Rightarrow Zn^{+2} + H_2O$$

As shown by equation, the degradation to ZnO dissolution in basic media is minimal at pH values greater than 6.0.

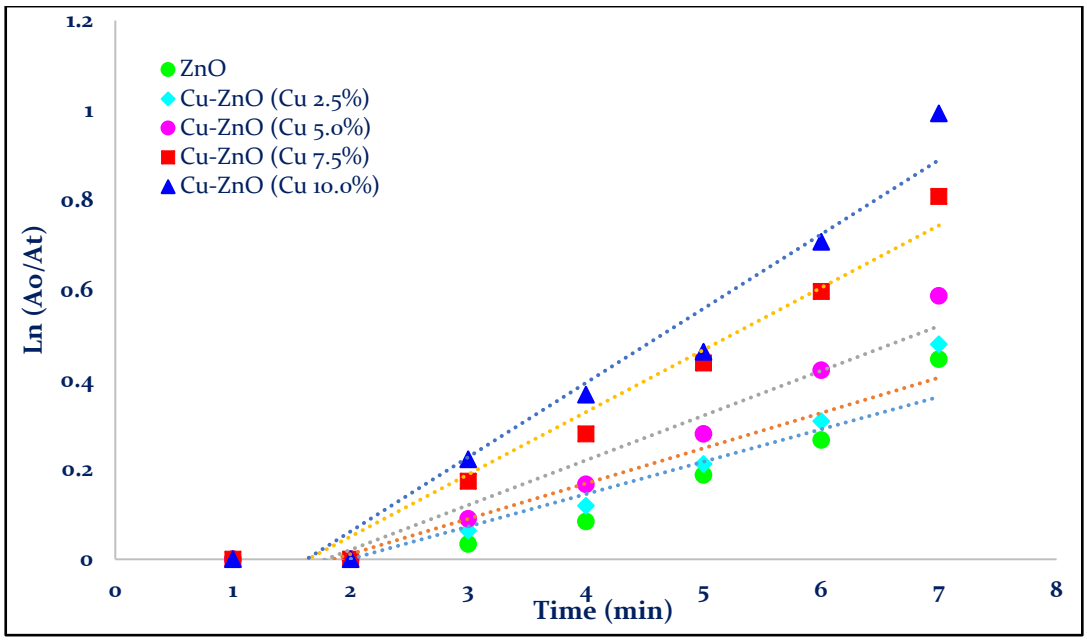

Fig. 17. Pseudo-first order kinetics of dye degradation under UV light.

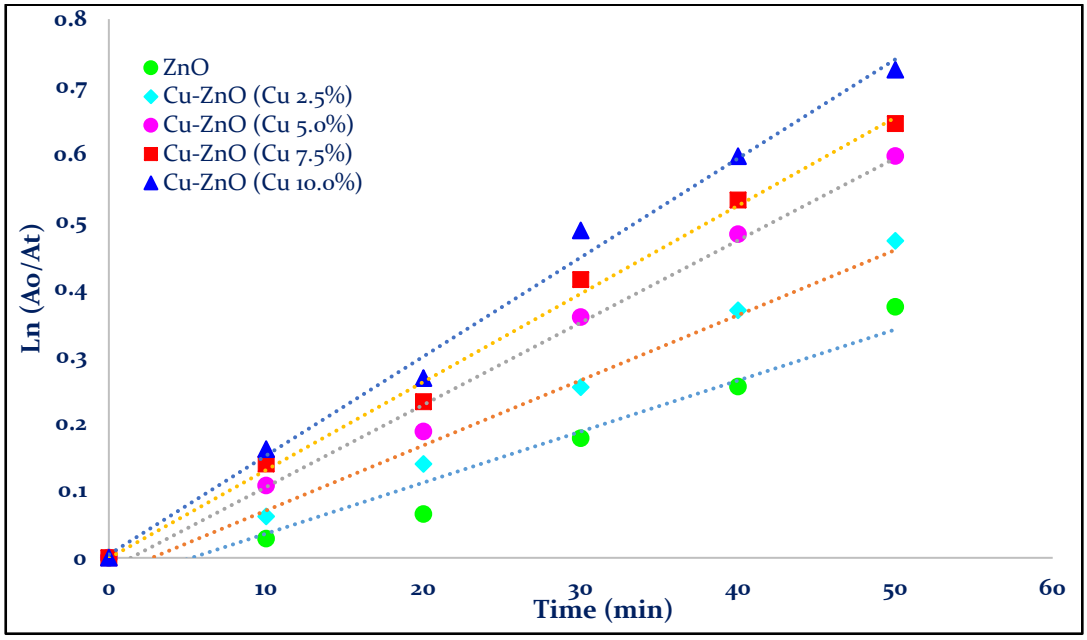

Fig. 18. Pseudo-first order kinetics of dye degradation in absence of light.

$$ZnO_{(s)} + 2OH^-_{(aq)} \Rightarrow ZnO_2^- + H_2O$$

The surface charge property of NCs, which is reliant on the pH point of zero charge, has an impact on how dye molecules adsorb to the surface of the photocatalyst. Thus, the catalytic surface would efficiently adsorb the organic anions of dye at pH 6.0, accelerating the degradation of dye on ZnO and Cu-ZnO NSs.

Hence after discussion, it is concluded that the synthesized photocatalyst $Zn_{1-x}Cu_xO$ ($x = 10.0$ %), showed maximum degradation as time or irradiation increases under solar radiations at optimum 6.0, while the synthesized photocatalyst ZnO NSs showed minimum degradation under same conditions.

It is proved from this research study, that on increasing the Cu metal content in ZnO crystal, the degradation was reached to its maximum level. It is also proved that the solar radiations used as irradiation source was found to be more effective for degradation of TD solution as compared to used other irradiation sources (UV-254 nm or absence of light).

4. Conclusion

ZnO nano particles & Cu doped ZnO NSs (Cu; 0.0 %, 2.5 %, 5.0 %, 7.5 % and 10.0 %) have been successfully prepared using SGAC approach. The crystalline structure of ZnO as well as the presence of Cu inside the crystalline structure were verified by the XRD data. The FT-IR results verified both the doping of Cu metal in ZnO structure as well as the production of the target materials. XRD analysis was used to establish the crystal structure and size, which showed the degree of

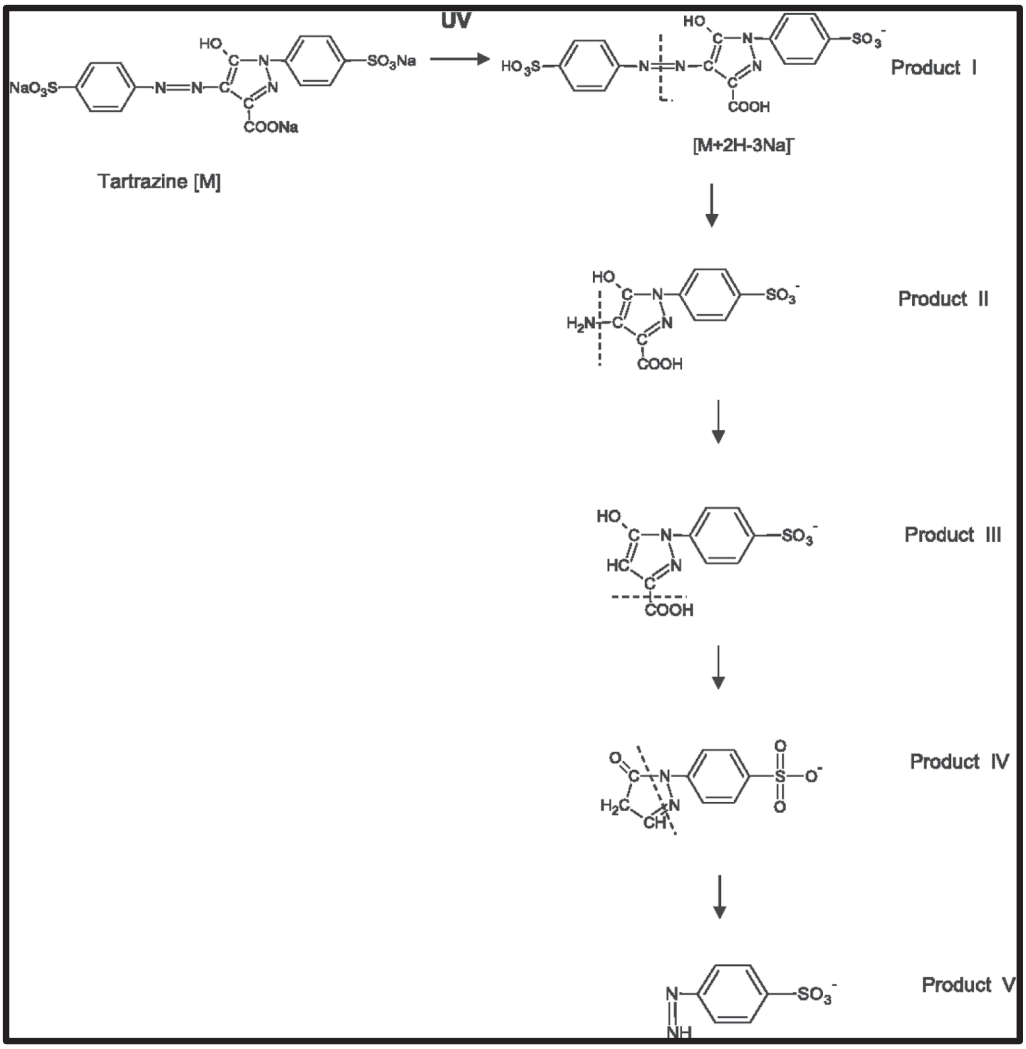

Fig. 19. Degradation mechanism of TD solution under UV Light irradiation.

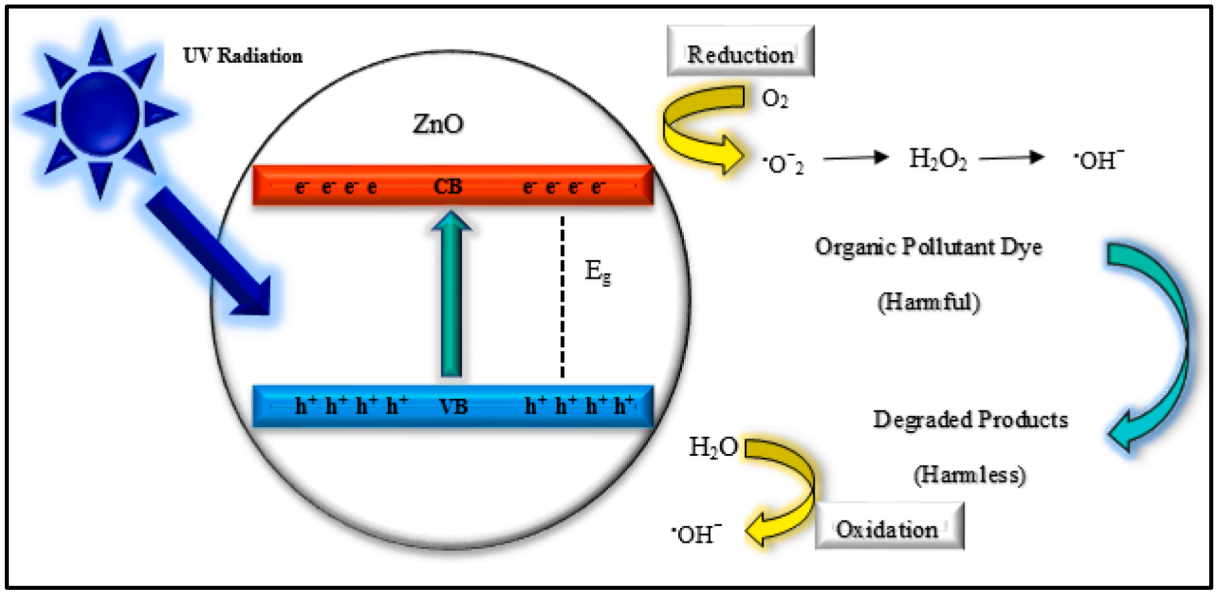

Fig. 20. Degradation of dye using ZnO NSs as photo catalyst under UV-254 nm light.

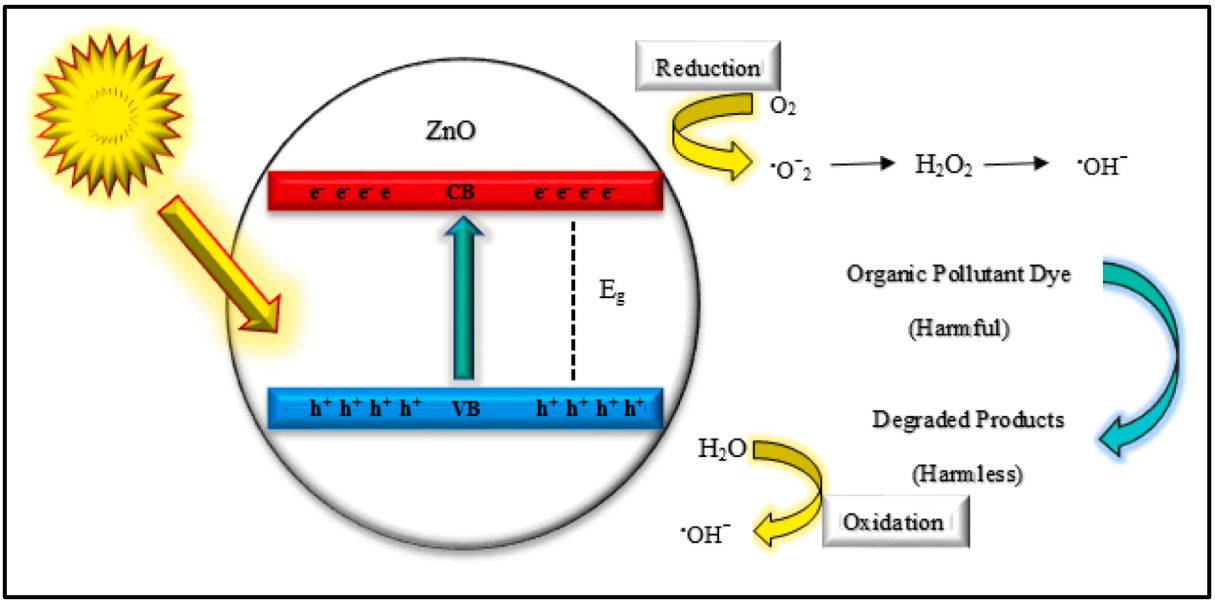

Fig. 21. Degradation of dye using ZnO NSs as photo catalyst under solar radiations.

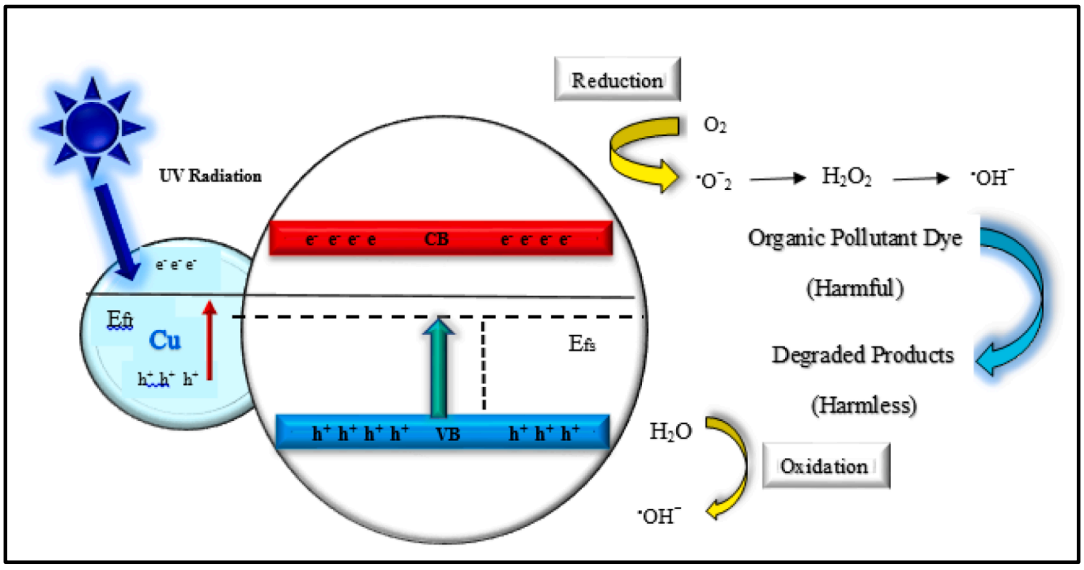

Fig. 22. Effect of Cu metal on Degradation of ZnO NSs under UV-254 nm light.

crystallinity decreased from 96.9 % to 92.8 % and crystal size increased from 33.8 nm to 174.9 nm. These results were found to be within acceptable ranges even after doping with Cu metal. As more Cu metal was incorporated into the ZnO structure, energy band gap of fabricated nanostructures found to be decreased from 3.36 to 3.20 eV. With the use of literature, it was determined that the electrical conductivity of synthesized materials increased as the Energy band gap reduced. Electrochemical properties were studies by CV analysis. There were no obvious redox peaks in the pure ZnO thin film CV curve. The 2.5 % Cu-ZnO nanostructure thin film, however, displayed reduction peaks at −0.316 V and 0.214 V as well as oxidation peaks at 0.252 V and −0.122 V. The 5.0 % Cu-ZnO nanostructure thin film displayed reduction peaks at −0.318 V and 0.214 V, as well as oxidation peaks at 0.262 V and −0.086 V. Finally, oxidation peaks at 0.266 V and −0.066 V, as well as reduction peaks at −0.342 V and 0.204 V, were seen in the 10 % Cu-ZnO nanostructure thin film. The Photocatalytic activity was also found to be optimized with 10.0 % Cu content under solar radiations. Under solar radiations, the samples showed their maximum degradation after complete process of 120 min which was up to 86.12 %. Under UV-254 nm, maximum degradation was found up to 72.16 % and in absence of light, degradation was upto 48.98 %. All synthesised Cu modified ZnO NSs had improved photo-induced catalytic degradation of organic pollutant dye and higher peak current when compared to pure ZnO. They also had improved relative electron transport. It was discovered that SGAC-produced products were much better to those previously reported in terms of quality and performance for the purposes intended.

Funding source

There was no funding sources provided for this study.

Declaration of Competing Interest

The authors declare that they have no known competing financial

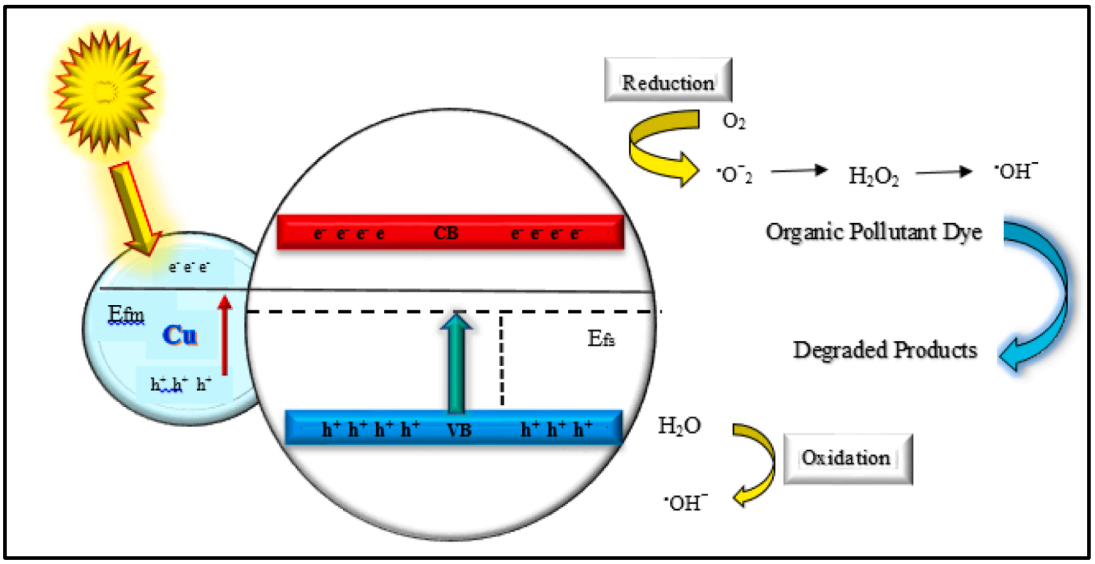

Fig. 23. Effect of Cu metal on Degradation of ZnO NSs under solar radiations.

interests or personal relationships that could have appeared to influence the work reported in this paper.

Data availability

The associated data to this work is available only on demand for scientific research purposes.

References

[1] F. Rehman, et al., Hydrothermal synthesis of copper doped zinc oxide nano composites to achieve optimum removal of organic pollutant dye from waste water following the photo catalytic degradation, J Nanomater Mol Nanotechnol 11 (6) (2022) 2.

[2] M. Fazal-ur-Rehman, Methodological trends in preparation of activated carbon from local sources and their impacts on production: a review, Chem. Int 4 (2018) 109–119.

[3] F.U. Rehman, et al., Development of nanosized ZnO-PVA-based polymer composite films for performance efficiency optimisation of organic solar cells, Eur. Phys. J. Plus 137 (10) (2022) 1105.

[4] F.U. Rehman, et al., Optimization of photo catalytic activity of ZnO nano composites by surface modification with Cu metal using facile hydrothermal approach, Iran. J. Catal. 12 (1) (2022) 25–44.

[5] M. Fazal-ur-Rehman, Novel applications of nanomaterials and nanotechnology in medical sciences-a review, J. Basic Appl. Sci. Res. 8 (4) (2018) 1.

[6] V. Dutta, et al., Bio-inspired synthesis of carbon-based nanomaterials and their potential environmental applications: a state-of-the-art review, Inorganics 10 (10) (2022) 169.

[7] A. Hamza, Y. Ozaki, M.S. Galadima, Photocatalytic degradation of methylene blue using natural ilmenite upgraded via HCl leaching: modelling and optimization, Appl. J. Envir. Eng. Sci. 5 (3) (2019) 252–262.

[8] R.-B. Lee, et al., Ilmenite: Properties and photodegradation kinetic on Reactive Black 5 dye, Chin. Chem. Lett. 28 (7) (2017) 1613–1618.

[9] D. Gupta, A. Boora, A. Thakur, T.K. Gupta, Green and sustainable synthesis of nanomaterials: recent advancements and limitations, Environ. Res. 231 (2023), 116316.

[10] X. Xie, P. Ge, R. Xue, H. Lv, W. Xue, E. Liu, Enhanced photocatalytic H2 evolution and anti-photocorrosion of sulfide photocatalyst by improving surface reaction: a review, Int. J. Hydrogen Energy 48 (63) (2023) 24264–24284.

[11] D. Rawat, A. Kumari, R.R. Singh, Synthesis and functionalization of magnetic and semiconducting nanoparticles for catalysis, Functionalized Nanomaterials for Catalytic Application (2021) 261–302.

[12] K. Pagar, et al., Bio-inspired synthesis of CdO nanoparticles using Citrus Limetta peel extract and their diverse biomedical applications, J Drug Deliv Sci Technol 82 (2023), 104373.

[13] O.I. Ismail, N.A. Rashed, Riboflavin attenuates tartrazine toxicity in the cerebellar cortex of adult albino rat, Sci. Rep. 12 (1) (2022), 19346.

[14] D. Neupane, Magnetocaloric Effect in Oxide Materials, The University of Memphis, 2022.

[15] A. Mancuso, G. Iervolino, Synthesis and application of innovative and environmentally friendly photocatalysts: a review, Catalysts 12 (10) (2022), 1074.

[16] E. Hannachi, Y. Slimani, M. Nawaz, R. Sivakumar, Z. Trabelsi, R. Vignesh, S. Akhtar, M.A. Almessiere, A. Baykal, G. Yasin, Preparation of cerium and yttrium doped ZnO nanoparticles and tracking their structural, optical, and photocatalytic performances, J. Rare Earths 41 (5) (2023) 682–688.

[17] Q.A. Moallem, H. Beitollahi, Electrochemical sensor for simultaneous detection of dopamine and uric acid based on a carbon paste electrode modified with nanostructured Cu-based metal-organic frameworks, Microchem. J. 177 (2022), 107261.

[18] E.F. Mohamed, G. Awad, Solar photocatalytic degradation of organic pollutants from indoor air using novel direct flame combustion based hollow nanocomposite of Pd/Anatase–Rutile TiO_2 mixed phase and evaluation of the biocompatibility, Adv. Powder Technol. 32 (7) (2021) 2555–2565.

[19] L. Ben Saad, L. Soltane, F. Sediri, Pure and Cu-doped ZnO nanoparticles: hydrothermal synthesis, structural, and optical properties, Russ. J. Phys. Chem. A. 93 (13) (2019) 2782–2788.

[20] K. Gherab, et al., Fabrication and characterizations of Al nanoparticles doped ZnO nanostructures-based integrated electrochemical biosensor, J. Mater. Res. Technol. 9 (1) (2020) 857–867.

[21] Y. Tang, M. Wang, J. Liu, S. Li, J. Kang, J. Wang, Z. Xu, Electro-enhanced sulfamethoxazole degradation efficiency via carbon embedding iron growing on nickel foam cathode activating peroxymonosulfate: mechanism and degradation pathway, J. Colloid Interface Sci. 624 (2022) 24–39.

[22] X. Wang, M. Ahmad, H. Sun, Three-dimensional ZnO hierarchical nanostructures: Solution phase synthesis and applications, Materials 10 (11) (2017) 1304.

[23] E.B. Aydın, G. Sığırcık, Preparations of different ZnO nanostructures on TiO_2 nanotube via electrochemical method and its application in hydrogen production, Int. J. Hydrog. Energy 44 (23) (2019) 11488–11502.

[24] M. Ahmad, J. Zhu, ZnO based advanced functional nanostructures: synthesis, properties and applications, J. Mater. Chem. 21 (3) (2011) 599–614.

[25] A. Sulciute, et al., ZnO nanostructures application in electrochemistry: influence of morphology, J. Phys. Chem. C 125 (2) (2021) 1472–1482.

[26] J. Liu, et al., Oriented nanostructures for energy conversion and storage, ChemSusChem: Chemistry & Sustainability Energy & Materials 1 (8–9) (2008) 676–697.

[27] J.L. Gomez, O. Tigli, Zinc oxide nanostructures: from growth to application, J. Mater. Sci. 48 (2013) 612–624.

[28] V. Parihar, M. Raja, R. Paulose, A brief review of structural, electrical and electrochemical properties of zinc oxide nanoparticles, Rev. Adv. Mater. Sci. 53 (2) (2018) 119–130.

[29] S. He, et al., Preparation and properties of ZnO nanostructures by electrochemical anodization method, Appl. Surf. Sci. 256 (8) (2010) 2557–2562.

[30] V. Vinitha, et al., Two is better than one: catalytic, sensing and optical applications of doped zinc oxide nanostructures, Emergent Mater 4 (5) (2021) 1093–1124.

[31] A.M. Kasumov, et al., Photocatalysis with the use of ZnO nanostructures as a method for the purification of aquatic environments from dyes, J. Water Chem. Technol. 43 (4) (2021) 281–288.

[32] H.I. Abdulgafour, T.A. Hassan, F.K. Yam, New Comparative Study of High-Sensitivity H_2 Gas Sensors at Room Temperature Based on ZnO NWs Grown on Si and PS/Si Substrates without Catalyst by Wet Thermal Evaporation Method, in: Journal of Physics: Conference Series, Vol. 2114, No. 1, IOP Publishing, 2021, p. 012087.